Acta Oceanol. Sin., 2021, Vol. 40, No. 11, P. 119–128
https://doi.org/10.1007/s13131-021-1767-5
http://www.aosocean.com
E-mail: ocean2@hyxb.org.cn

Mechanisms for the link between onset and duration of open water in the Kara Sea

Chunming Dong[1], Hongtao Nie[1]*, Xiaofan Luo[1], Hao Wei[1], Wei Zhao[1]

[1] School of Marine Science and Technology, Tianjin University, Tianjin 300072, China

Received 27 October 2020; accepted 28 November 2020

Abstract

The sea ice conditions in the Kara Sea have important impacts on Arctic shipping, oil and gas production, and marine environmental changes. In this study, sea ice coverage (C_R) less than 30% is considered as open water, its onset and end dates are defined as T_{open} and T_{close}, respectively. The sea ice melt onset (T_{melt}) is defined as the date when ice-sea freshwater flux initially changes from ice into the ocean. Satellite-based sea ice concentration (SIC) from 1989 to 2019 shows a negative correlation between T_{open} and T_{close} (r = –0.77, p < 0.01) in the Kara Sea. This phenomenon is also obtained through analyzing the hindcast simulation from 1994 to 2015 by a coupled ocean and sea-ice model (NAPA1/4). The model results reveal that thermodynamics dominate the sea ice variations, and ice basal melt is greater than the ice surface melt. Heat budget estimation suggests that the heat flux is significant correlated with T_{open} (r = –0.95, p < 0.01) during the melt period (the duration of multi-year averaged T_{melt} to T_{open}) influenced by the sea ice conditions. Additionally, this heat flux is also suggested to dominate the interannual variation of the heat input during the whole heat absorption process (r = 0.81, p < 0.01). The more heat input during this process leads to later T_{close} (r = 0.77, p < 0.01). This is the physical basis of the negative correlation between T_{open} and T_{close}. Therefore, the duration of open water can be predicted by T_{open} and thence support earlier planning of marine activities.

Key words: sea ice, open water onset, duration of open water, heat budget, Kara Sea

Citation: Dong Chunming, Nie Hongtao, Luo Xiaofan, Wei Hao, Zhao Wei. 2021. Mechanisms for the link between onset and duration of open water in the Kara Sea. Acta Oceanologica Sinica, 40(11): 119–128, doi: 10.1007/s13131-021-1767-5

1 Introduction

Arctic sea ice extent has decreased dramatically in the past 40 years (Cavalieri and Parkinson, 2012; Lindsay and Schweiger, 2015; Stroeve and Notz, 2018). The summer sea ice has decreased significantly, especially in the marginal seas of the Arctic (Onarheim et al., 2018; Simmonds, 2015). Continued sea ice loss will make the Arctic Ocean increasingly accessible for oil and natural gas exploration and development, marine transportation, tourism, and other activities (Navy's Task Force Climate Change, 2014). Therefore, it is very important to understand the regularity of the onset and duration of open water every year to arrange production in advance and to ensure the safety of marine activities. The Kara Sea (Fig. 1) is rich in oil and gas resources and is a key sea area of the Northeast Passage (Aksenov et al., 2017; Bird et al., 2008; Gautier et al., 2009). Meanwhile, the Kara Sea is one of the regions that most dramatically impacted by global warming in the Arctic Ocean (Kim et al., 2016). The prediction of open water duration in this region is urgently required.

Previous studies have shown that seasonal changes in sea ice cover not only represent the response of the surface energy budget to climate (Blanchard-Wrigglesworth et al., 2011; Markus et al., 2009) but also result from ocean dynamic and thermodynamic effects (Maslanik et al., 1996; Wang et al., 2019b). The average annual melt and freeze onset dates of the Arctic Ocean are significantly correlated with the Arctic Oscillation (AO) index. During the high-index AO, sea ice in most parts of the Arctic began to melt earlier and freeze later (Belchansky et al., 2004; Johnson and Eicken, 2016; Lebrun et al., 2019; Stammerjohn et al., 2012; Stroeve et al., 2016). Winter cyclone wind field responding to high-index AO enhances the divergence of ice in the eastern Arctic (Rigor et al., 2002). These processes result in more open water, thin ice or leads, leading to decreased surface albedo and increased heat flux into the sea (Lei et al., 2016; Perovich et al., 2007a). Additionally, the increased sea surface air humidity and temperature trigger the efficient feedback of the atmosphere-ocean-sea ice system (Ikeda et al., 2001; Mysak and Venegas, 1998), favoring a longer duration of open water in summer (Curry et al., 1995; Flanner et al., 2011; Screen and Simmonds, 2010; Serreze and Barry, 2011).

However, the sea ice melt onset in the marginal seas of the Arctic Ocean responds differently to AO. Earlier melt onset in the Laptev, East Siberian, and the Chukchi Sea regions was found to be associated with a positive AO index (Belchansky et al., 2004; Bliss and Anderson, 2014), while the melt onset in the Beaufort Sea and the Barents Sea is primarily controlled by ocean circulation heat transport (Lien et al., 2017; Serreze et al., 2016). Owing to the strong reliance of melt onset on local weather conditions, the Kara Sea is the most highly variable sub-region of the Arctic Ocean (Bliss and Anderson, 2014). Melt onset in the Kara Sea does not reveal an obvious relationship with climate factors, making it difficult to predict. Therefore, determining an independent indicator from melt onset for open water evolution is significant to meet practical demands.

It is difficult to distinguish the contributions of dynamic and

Foundation item: The National Key Research and Development Program of China under contract No. 2016YFC1401401; the National Natural Science Foundation of China under contract Nos 41630969, 41941013 and 41806225.
*Corresponding author, E-mail: htnie@tju.edu.cn

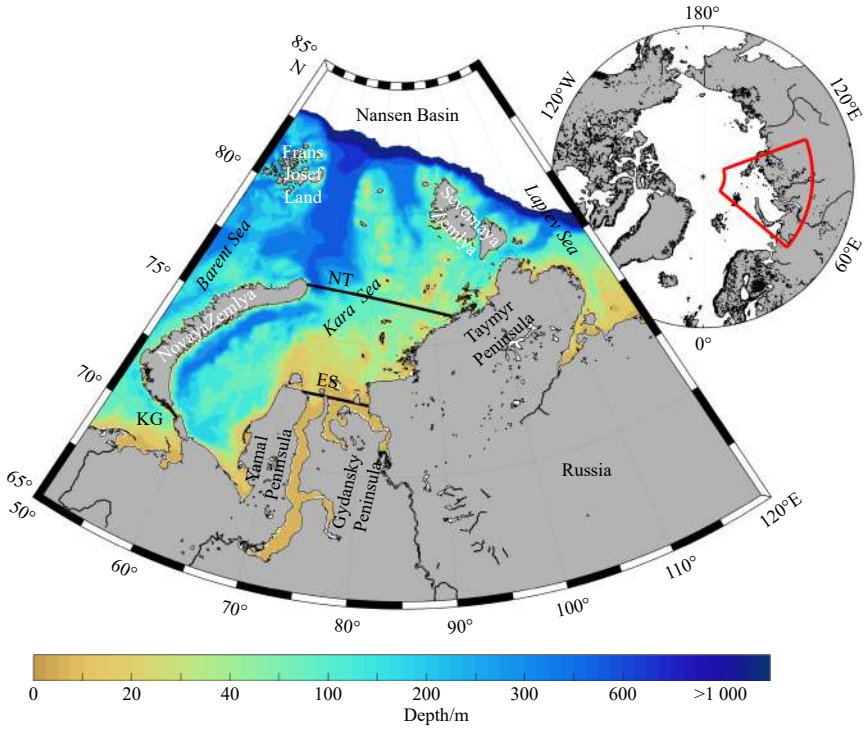

Fig. 1. Location and bathymetry of the Kara Sea (the topography data came from the ORCA025 developed for the DRAKKAR project, https://www.drakkar-ocean.eu/global-models/orca025). The study region is bounded by three sections (thick black lines), Kara Gate (KG), Novaya Zemlya-Taymyr Peninsula (NT), Estuaries of Ob and Yenisei (ES).

thermodynamic processes to water column heat changes only through the correlations among wind, runoff, sea surface temperature, and sea ice (Chen and Zhao, 2017; Duan et al., 2019a; Leifer et al., 2018). The underlying mechanism linking sea ice melting and freezing is required to be analyzed with a coupled ocean and sea-ice model that includes the feedback process. Some questions regarding the causes of ice variation remain unanswered; for example, does the atmosphere-forced ice surface melt regulate the primary features of ice variation? Which period is more crucial for interannual variations of heat budget and thence the ice volume variations? Additionally, in the Chukchi Sea, Pacific heat influx through the Bering Strait is equivalent to the solar radiation (Perovich et al., 2007b; Woodgate et al., 2015), indicating that the lateral heat flux has a significant impact on the interannual variations in sea ice (Wang et al., 2019a). In the Kara Sea, the role of lateral heat flux, including runoff from the Ob and Yenisei rivers and the inflow from the Barents Sea remains unclear. Quantitative analysis based on the combination of sea ice and heat budget is helpful for further understanding the physical mechanism of the atmosphere-ocean-sea ice feedback in different periods of the year.

Using satellite-based sea ice concentration (SIC) and a coupled ocean and sea-ice model simulations, this study explores interannual variations in the open water onset and end date in the Kara Sea. Afterwards, heat budgets during the ice melt and open water period are estimated. Finally, the underlying mechanism linking sea ice melting and freezing is clarified and the prediction scheme for open water duration is obtained.

2 Data and methods

2.1 *Data sources*

The daily satellite remote sensing data set from 1989 to 2019, with a horizontal resolution of 25 km, is the Climate Data Record (CDR) from Nimbus-7 SMMR and DMSP SSM/I-SSMIS Passive Microwave Sea Ice Concentration, created by the National Snow and Ice Data Centre (NSIDC) of the USA National Oceanic and Atmospheric Administration (NOAA) (Meier et al., 2017). The CDR algorithm output is a rule-based combination of ice concentration estimates from two well-established algorithms: the National Aeronautics and Space Administration (NASA) Team (NT) algorithm (Cavalieri et al., 1984) and NASA Bootstrap (BT) algorithm (Comiso, 1986).

The coupled ocean and sea-ice model (NAPA1/4) is version 3.6 of the Nucleus for European Modelling of the Ocean (NEMO 3.6) (Madec, 2008; NEMO book, available at https://www.nemo-ocean.eu/wp-content/uploads/NEMO_book.pdf) and version 3 of Louvain-la-Neuve Sea Ice Model (LIM3) (Rousset et al., 2015; Vancoppenolle et al., 2009). The horizontal model grid is derived from the ORCA global three-pole grid (Madec and Imbard, 1996) (DRAKKAR, https://www.drakkar-ocean.eu/what-is-drakkar). The model covers the North Atlantic-North Pacific-Arctic Oceans (NAPA) with a nominal horizontal resolution of (1/4)° in latitude/longitude and reproduces the main observed features of ocean and sea ice variations during 1994–2015. The configuration and evaluation of the coupled ocean and sea-ice model are detailed in Luo et al. (2019) and Zhang et al. (2020).

LIM3 in the NAPA1/4 model is a C-grid dynamic-thermodynamic sea ice model with thickness, enthalpy, salinity, and age distributions. It includes a series of ice thickness categories, that can better simulate the rapid formation and loss of thin ice and the physical transition process from thin ice to thick ice caused by sea ice overlap and ridge formation (Uotila et al., 2017). The melting of sea ice is divided into two parts: surface and basal melt. The widely used LIM3 in the Arctic does not explicitly consider the lateral melt, but some implicit lateral melting is accounted for by the melt of thin ice (Bitz et al., 2001).

2.2 *Evaluation of model simulated sea ice concentration*

The NAPA1/4 model reproduces the consistent variation in sea ice in the Kara Sea with that displayed by the CDR data set. The spatial distribution of SIC from May to October is based on the CDR data set (Figs 2a–f) and the NAPA1/4 simulation (Figs 2g–l) averaged over 1994 to 2015. Both data sets suggested that sea ice first melted in the regions of warm water inflow, including the estuaries, the Kara Strait, and the northern part of Novaya Zemlya. Subsequently, the ice melting area gradually expanded, and the SIC in the southern and southwestern regions gradually decreased. In July, the ice-free area first appeared in the estuaries, and the ice edge retreated from south to north and from west to east. By September, the sea ice covered area reached the minimum value, and the focus area bounded by the Kara Strait, the estuaries, and the northern side of the Novaya Zemlya-Taymyr Peninsula, corresponding to KG, ES, NT sections, is completely ice-free. In October, sea ice expanded from high latitudes to low latitudes and then extended to the southwestern Kara Sea. Seasonal variations in sea ice concentration indicate that compared to freezing, melting is a relatively slow process in the Kara Sea. Further statistical analysis shows that the modeled seasonal variation in the regional averaged SIC in each year from 1994 to 2015 has a significant correlation coefficient of greater than 0.95 with the CDR data set (Fig. 2m).

2.3 *Methods*

In this study, sea ice coverage is used to analyze the changes in sea ice and is calculated through the method introduced by Duan et al. (2019b).

$$\mathrm{SIA} = \int_S e_i s_i c_i \mathrm{d}S, \begin{cases} e_i = 0 & c_i < 15\% \\ e_i = 1 & c_i \geqslant 15\% \end{cases}, \tag{1}$$

$$C_R = \mathrm{SIA}/S, \tag{2}$$

where C_R is the sea ice coverage (%); SIA is the sea ice cover area; c_i, s_i, and e_i are the SIC, area, and weight coefficient in each grid; S is the total area of the focus region. The ice concentration of 15% is considered as the sea ice edge (Comiso and Nishio, 2008; Ogi et al., 2008).

To quantify the interannual variations in the open water evolution in the Kara Sea (Fig.1), C_R = 30% is used as the threshold of the start and end dates of open water (Stroeve et al., 2016; Serreze et al., 2016; Wang et al., 2019a). The date when C_R reaches and remains below the threshold is defined as the start date of the open water (T_{open}); the earliest date when C_R is larger than and remains above the threshold after T_{open} is defined as the end date of the open water (T_{close}). The period between T_{open} and T_{close} is defined as the duration of open water (DOW).

For the heat balance of the water column, the vertical heat flux at the sea surface (including the surfaces of open water and the leads, and the ice-sea interface) in the study area is the sum of net solar radiation, net longwave radiation, and sensible and latent heat fluxes. The ice-sea freshwater flux, sea surface net heat flux, the ice surface/basal melt rates are included in the model output. The calculation method is clearly described in the LIM3 instruction (available at http://www.climate.be/users/lecomte/LIM3_users_guide _2012.pdf).

The lateral net heat flux includes the heat exchange through KG, ES, and NT sections in Fig. 1, and is calculated following the method proposed by Woodgate (2018):

$$Q_{\mathrm{lateral}} = \rho C_{\mathrm{w}} \iint (\theta - \theta_{\mathrm{ref}}) v \mathrm{d}x\mathrm{d}z + \rho C_{\mathrm{w}} \iint (\theta - \theta_{\mathrm{ref}}) u \mathrm{d}y\mathrm{d}z, \tag{3}$$

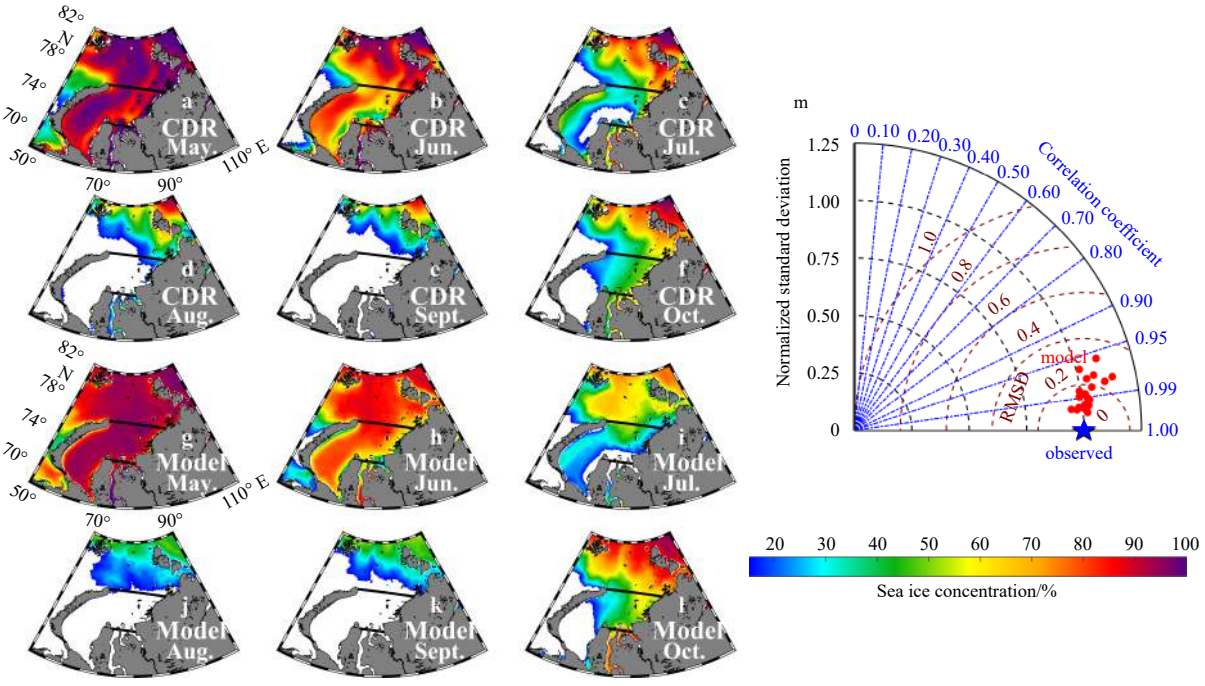

Fig. 2. Spatial distributions of sea ice concentration from May to October from the CDR data set (a–f) and simulation results of NAPA1/4 (g–l), averaged over 1994–2015 in the Kara Sea; and the Taylor diagram showing normalized standard deviations (distant from the origin), correlations (azimuth angle), and bias removed RMS differences (Euclidian distance from the reference point) between NAPA 1/4 and the CDR data set (m). The reference point (blue star) applies to all satellite observed values. The red dots represent 5 d averaged time series in each year from 1994 to 2015.

where $Q_{lateral}$ is defined as the lateral heat flux; θ_{ref} is the referential temperature (–1.9°C); θ (°C) is the seawater temperature; ρ is the density of seawater (1 023 kg/m^3); C_ω is the specific heat capacity of water which is the function of temperature, salinity and pressure; and v (m/s) and u (m/s) are the north–south and east–west components of the velocity, respectively.

3 Results and discussion

3.1 *Interannual variations of T_{open} and T_{close}*

Based on the CDR data set, the daily C_R overlapped with T_{open} and T_{close} from 1989 to 2019 is shown in Fig. 3a. A strong correlation was found between T_{open} and T_{close} with the coefficient r = –0.77 (p < 0.01). While T_{close} in the previous year showed a weak correlation with the following T_{open} (r = –0.43, p < 0.01). This suggests a significant impact of T_{open} on T_{close} in one year, i.e., early (late) opening and late (early) closing (Lei et al., 2015), while T_{close} has a limited impact on the next year T_{open}. Satellite data shows that T_{open} and T_{close} of the sea ice have a linear trend of approximately –1.0 d/a and 1.0 d/a, respectively, and the DOW has an increasing trend of interannual change. In 2011 and 2012, T_{open} was relatively earlier and together with a longer duration of open water. In 1998 and 1999, heavy ice existed in the Kara Sea, the T_{open} was delayed, and the duration of open water was shorter.

NAPA1/4 reproduced similar interannual variations in open water evolution from 1994 to 2015 in this region (Fig. 3b). Overall, T_{open} derived from NAPA1/4 is slightly earlier (three days on average) than that derived from the CDR data set. The two have a correlation of r = 0.92 (p < 0.01). In terms of T_{close}, the two time series also matches well (r = 0.89, p < 0.01). T_{open} and T_{close} based on NAPA1/4 show a correlation of r = –0.67 (p < 0.01), indicating that T_{open} arrives earlier and T_{close} becomes later. Both the NAPA1/4 and CDR data set reveal that the duration of open water is gradually extended with time. This agrees with the phenomenon that the sea ice cover in the Arctic Ocean has fallen sharply and the duration of the ice-free season has increased (Barnhart et al., 2016).

3.2 *Controls on sea ice variations*

The variations in sea ice are influenced by dynamic and thermodynamic processes (Hu et al., 2018; Lindsay and Zhang, 2005; Rigor et al., 2002). The thermodynamic process directly affects the freezing and melting of sea ice. The dynamic process mainly affects the sea ice movement, breakage, ridge, leads, and then affects the sea ice distribution and thermal changes. Based on NAPA1/4, the contributions of thermodynamic and dynamic processes on the ice volume averaged over 1994–2015 were estimated (Fig. 4). From January to May, the Kara Sea is ice covered, the thermodynamics leads to the increase of sea ice volume, while the dynamics make the sea ice volume decrease. At the beginning of June, thermodynamic effects shift from positive to negative and induce ice decay. The total ice decay, driven by thermodynamics, peaks in early July. In early October, sea ice grows gradually, and the contribution of thermodynamics changes from negative to positive. During the warm months (June–October), the total ice variation (–1.08 ± 0.93) cm/d matches well with thermodynamics indicated ice variation (–1.09 ± 0.97) cm/d. In the other months, thermodynamics remains prevalent (1.21 ± 0.59) cm/d, but the dynamic effect increases by 24% (–0.39 ± 0.26) cm/d as compared to warm months (0.02 ± 0.39) cm/d. During the cold months, the dynamic processes play a role in ice export, which is consistent with the finding from Kern et al. (2005). This is likely accountable for the weak correlation between T_{close} and the following T_{open}. The contribution ratios of dynamic and thermodynamic processes were quantitatively analyzed through the sea ice growth and decay rates. Using

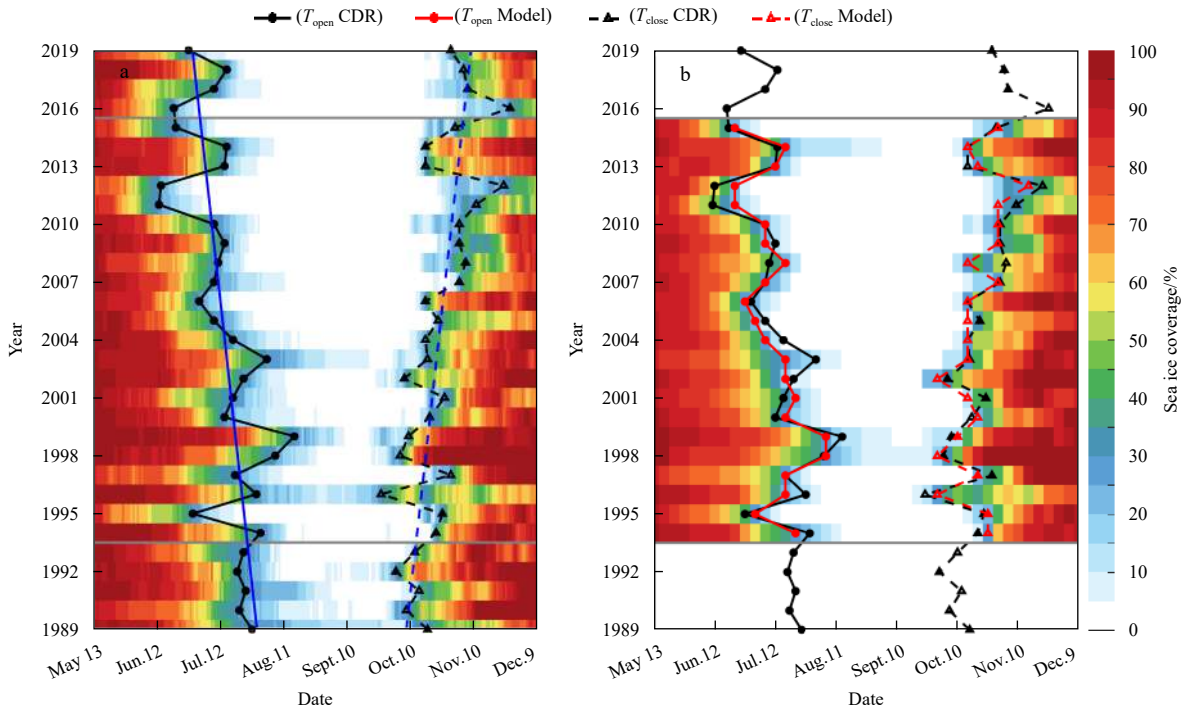

Fig. 3. Variations in C_R based on the climate data record (CDR) data set (a) and NAPA1/4 model (b). The black and red lines in both subfigures denote the T_{open} (solid) and T_{close} (dashed), respectively. The blue lines represent the linear trend of T_{open} and T_{close} based on the CDR.

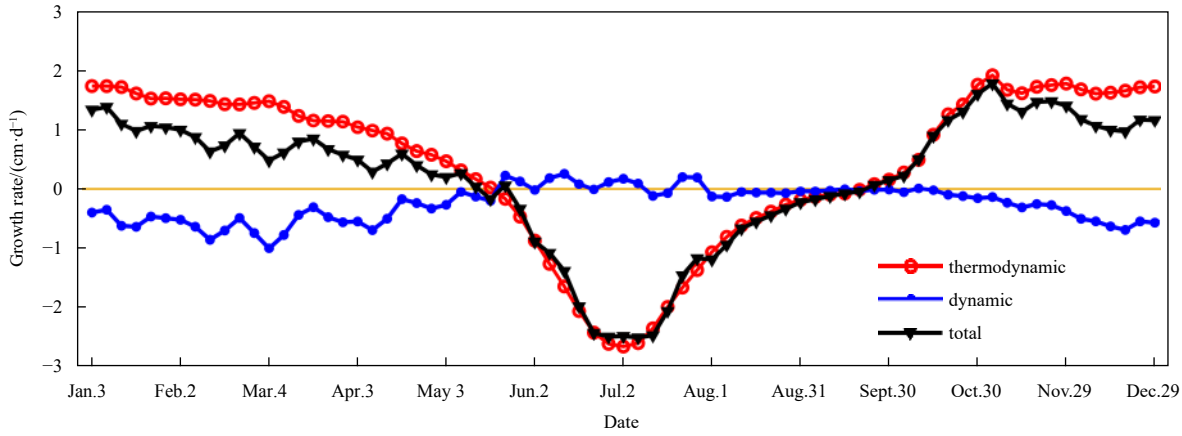

Fig. 4. Annual cycle of sea ice growth and decay rate of ice thickness averaged over 1994–2015 based on NAPA1/4. The negative (positive) value indicates the sea ice decay (growth) rate. Lines with the red circle, blue dot and black triangle represent the thermodynamic, dynamic process and the total contributions to ice variation, respectively.

the dynamics as an example, the contribution ratio is calculated as follows:

$$\text{contribution ratio} = \frac{|\text{dynamics}|}{|\text{dynamics}| + |\text{thermodynamics}|} \times 100\% . \quad (4)$$

During June–October and the remaining months, the contribution ratios of dynamics are 2% and 24%, respectively. Annually, the contribution ratios of thermodynamics and dynamics are 63% and 37%, respectively, suggesting that thermodynamics are the principal forces causing ice variations in the Kara Sea (Polyakov et al., 2003).

Hence, sea ice volume changes due to thermodynamics are focused on. Figure 5a shows the multi-year averaged surface, basal melting rate, and ice-sea freshwater flux in the Kara Sea in 1994–2015. The ice-sea freshwater flux can be regarded as the change of sea ice volume caused by the thermodynamic process, and its size and variation are consistent with the total melting rate of sea ice. The negative (positive) values of ice-sea freshwater flux denote the total ice melting (formation). The sea ice melt onset (T_{melt}) is defined as the date when ice-sea freshwater flux initially changes from ice into the ocean. The duration of multi-year averaged T_{melt} to T_{open} is defined as the ice melt period (May 21 to July 15) and the duration from T_{open} to T_{close} is defined as the open water period (July 16 to October 22), based on the multi-year averaged result. Before the melt period, ice basal melt (< –0.01 cm/d) already exists (Fig. 5b). In early July, the ice-sea freshwater flux reaches its peak value of approximately –2.65 cm/d. This phenomenon occurs in the melt period. During this period, the mean basal melt rate is (–1.13 ± 0.54) cm/d, 79% larger than surface melt (–0.63 ± 0.37) cm/d . Averaged over the open water period, the basal melt accounts for 82% of the total melt.

Overall, the total ice melting during the two periods is primarily contributed by the ice basal melt (76%). Ice surface melt plays a minor role in ice variation. This indicates that atmosphere influences on the ice surface processes alone cannot explain ice variation, while oceanic heat fluxes that are influenced by atmosphere forcing and oceanic transport play a key role in ice basal processes and ice variation. Thus, more attention should be paid to oceanic heat fluxes.

3.3 *Heat budget in the ice melt and open water periods*

The heat budget in the Kara Sea includes the vertical heat flux

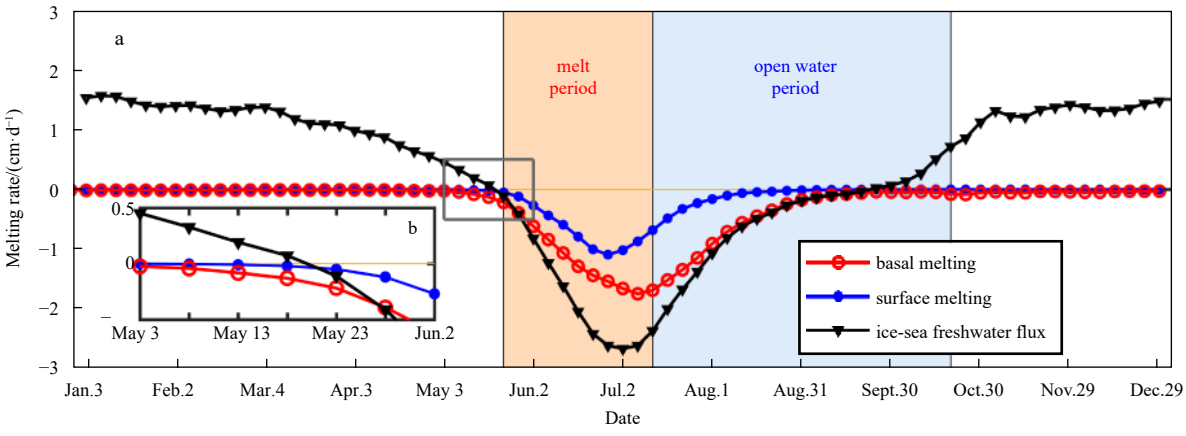

Fig. 5. Annual cycle average of the sea ice surface melting rate (blue dot), basal melting rate (red circle), and freshwater flux from ice to the ocean (black triangle) in the Kara Sea averaged over 1994–2015 (a); and melting rates from May 3rd to June 2nd (box outlined in gray in a) (b). These variables are calculated from NAPA1/4 (see the guide book available at http://www.climate.be/users/lecomte/LIM3_users_guide_2012.pdf). The negative (positive) value indicates the sea ice melting (formation) rate.

through the sea surface and the lateral heat flux through the NT, KG and ES sections. Figure 6 shows the annual-cycles of the sea surface temperature (SST) and heat fluxes in the study region. Before the melt period, the lateral heat flux entering the Kara Sea is principally used in the ice/water phase transition and does not make SST rise. In early May, the ocean absorbs vertical heat flux through the sea surface to promote ice basal melt (Fig. 5b). During the melt period, the vertical heat flux through the ice surface increases rapidly, further accelerating the melting of the ice basal (Fig. 5a) and the increase in SST. During the open water period, the lateral heat flux continues to increase, and the vertical heat flux decreases gradually from August owing to seasonal solar radiation changes. At the end of August, the SST reaches a peak value higher than 3°C. In September, the vertical heat flux changes from positive to negative, the ocean surface begins to release heat to the atmosphere and the decreases. Until late October, the open water is covered by ice.

In general, when sea ice melts to form thin ice or open water, it is difficult to distinguish the influence of lateral inflow on sea ice from that of local solar radiation, temperature, wind, and other factors (Stroeve et al., 2014; Wang et al., 2019b). Although the Kara Sea is more closely connected with rivers and the Barents Sea (Dmitrenko et al., 2015; Osadchiev et al., 2017), the lateral flux plays a minor role in the heat budget. This is quite different from the lateral inflow controlled by continental shelf sea, such as the Chukchi Sea (Wang et al., 2019a). Compared with lateral heat flux, vertical heat flux contributes 96% and 79% of the heat budget in the water column during the melt and open water period, respectively.

3.4 *Linkage of interannual variations in T_{open} and T_{close}*

The total heat flux, i.e., the summation of net vertical and lateral heat fluxes is essential in the ice melt and open water periods. The SIC during the melt period can reflect the macro effects of the local weather process. The SIC and total heat flux during the melt period have opposite interannual variations with T_{open} as shown in Fig. 7, with correlation coefficients of $r = -0.91$ ($p < 0.01$) and $r = -0.95$ ($p < 0.01$), respectively. The results show that sea ice conditions influence the variations in heat absorption during the melt period. More leads and thin ice enhance the heat flux, decrease surface albedo, and accelerate the melting through positive feedbacks (Markus et al., 2009; Rigor et al., 2002; Zhang et al., 2000), making the T_{open} earlier. Conversely, higher SIC delays the date of sea ice retreat, leading to a later T_{open}. Therefore, the net heat flux accumulated during the melt period has a great effect on the formation of the open water under the influences of sea ice conditions.

Figure 8 shows the interannual variations between total net heat flux and T_{close} during the melt period and the open water period. The mean value and standard deviation of the heat budget during the two periods are $(1.47 \pm 0.44) \times 10^{20}$ J and $(1.10 \pm 0.36) \times 10^{20}$ J, respectively. T_{close} is significantly correlated with net heat flux during the melt period ($r = 0.66$, $p < 0.01$), but without an obvious relationship with that during the open water

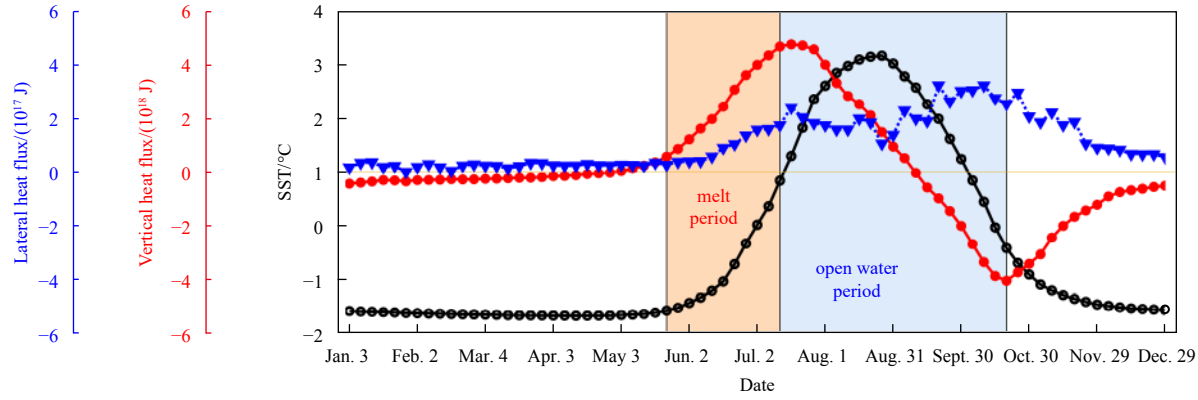

Fig. 6. Annual cycles of regional mean sea surface temperature (black dot), the lateral (blue triangle) and vertical (red dot) net heat flux averaged over 1994–2015 based on NAPA1/4. Positive (negative) values denote heat absorption (release).

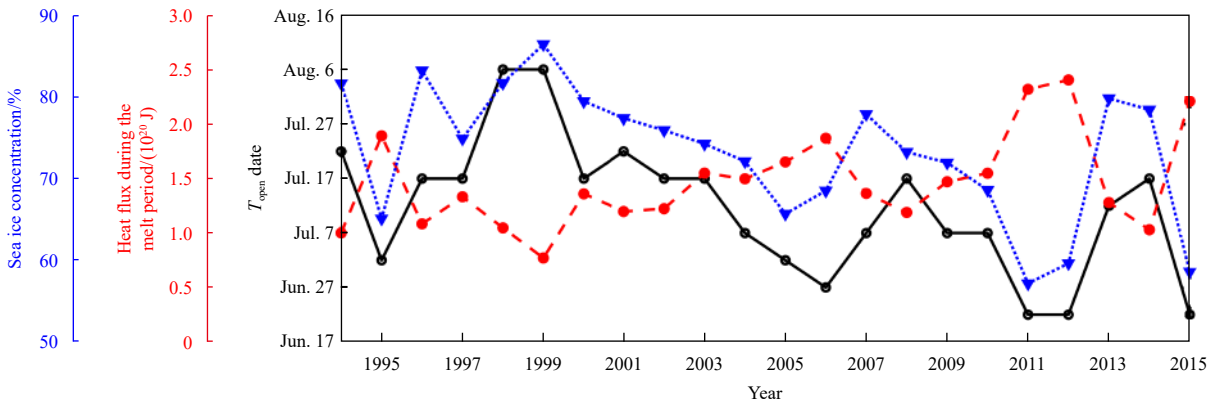

Fig. 7. Interannual variations in sea ice concentration (blue triangle), T_{open} (black dot), and accumulated heat flux during the melt period (red dot) based on NAPA1/4 in the Kara Sea.

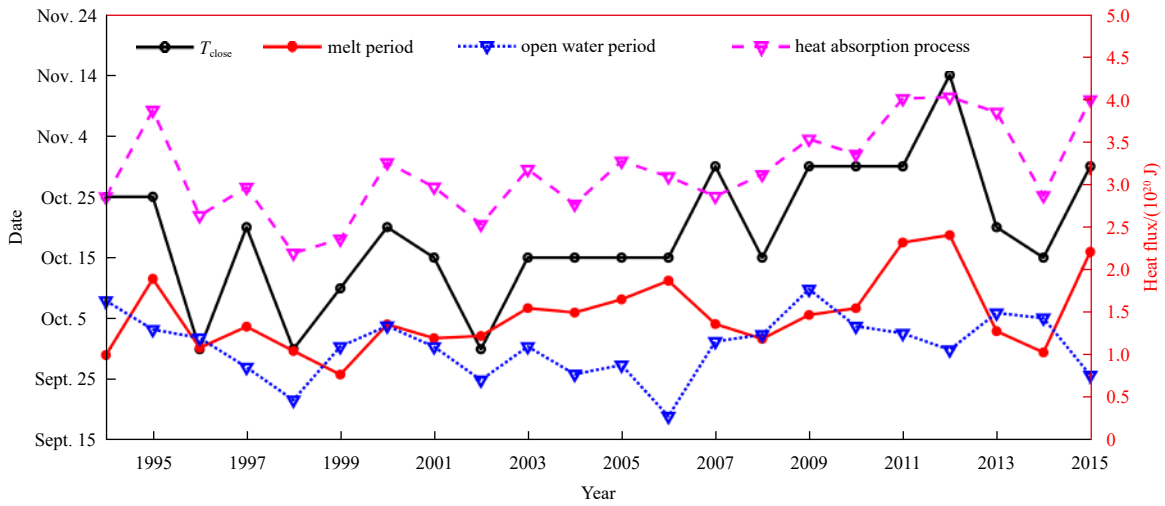

Fig. 8. Interannual variations in T_{close} (black circle), accumulated heat flux during the melt period (red dot), the open water period (blue triangle) and the heat absorption process (magenta triangle) based on NAPA1/4 in the Kara Sea.

period ($p > 0.05$). While during the first half of the open water period, the water column keeps gaining heat (Fig. 6). The accumulated heat during the whole heat absorption process (including the melt period and the first half of the open water period) shows significant correlations with T_{close} ($r = 0.77$, $p < 0.01$), indicating that more heat input during this process results in the later freezing date. In addition, the heat flux during the melt period is also correlated ($r = 0.81$, $p < 0.01$) with and dominates the interannual variation of the heat input during the whole heat absorption process, and therefore can be a good indicator of DOW afterwards.

4 Linkage between DOW and T_{open}

Sea ice conditions during the melt period influence the sea ice albedo positive feedback mechanism, resulting in an interannual variation in seawater heat absorption, which in turn affects the formation and DOW. Least-squares regression analysis shows the two time series T_{open} and DOW have a coefficient of determination (R^2) as high as 0.89 significance at the 95% confidence level (Fig. 9a). During 1989–2019, there is a lengthening of DOW, as well as earlier T_{open}. The relationship between T_{close} and DOW shows a significant correlation coefficient of $r = 0.94$ ($p < 0.01$). The empirical formula for the prediction of DOW in the Kara Sea is obtained as follows:

$$\mathrm{DOW} = -1.72T_{open} + 177.15. \quad (5)$$

The earliest open date of the Kara Sea is June 13; thus, the prediction formula considers June 1 as the first day of T_{open}, and T_{open} represents the number of days relative to the end of May. The relationship between T_{open} and DOW based on the CDR data set has been detrended by removing the long-term linear trend in the Kara Sea (Fig. 9b) still presents a significant correlation coefficient of $r = -0.91$ ($p < 0.01$). Using this regression relationship, the predicted DOW agrees well with CDR derived DOW. Assuming the latter as is accurate, a prediction using T_{open} and the above regression relationship provides a maximum absolute error of 9 days; the mean predicted DOW during 1989–2019 is equal to the observation values. This prediction scheme is practical and helpful for supporting the planning of marine activities in the Kara Sea.

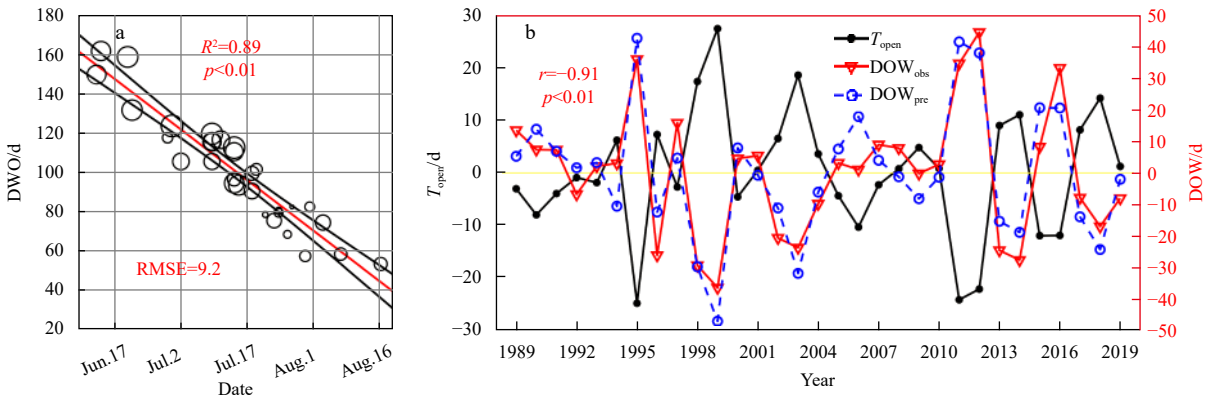

Fig. 9. Relationship between T_{open} (black dot) and duration of open water (DOW) of the Kara Sea derived from the CDR data set. a. Scatter diagram of DOW versus T_{open}, with their linear regression shown by the red line and 95% confidence bounds shown by the black lines. The sizes of open circles increase from 1989 to 2019. b. Detrended time series from 1989 to 2019. The red triangle and blue circle lines denote CDR derived DOW (DOW_{obs}) and predicted DOW (DOW_{pre}), respectively.

5 Conclusions

Satellite sea ice concentration in 1989–2019 identifies a strong negative correlation (r = –0.77, p < 0.01) between open water onset and reclose (denoted as T_{open} and T_{close}, respectively) in the Kara Sea. A coupled ocean and sea-ice model (NAPA1/4) reproduces the interannual variations. Based on NAPA1/4, this study estimated the relative contributions of thermodynamics and dynamics to sea ice variation. The results suggest that thermodynamics are the prevalent forces influencing the sea ice variations in the Kara Sea. We further analyzed the sea ice volume changes due to thermodynamics and separated the evolution of sea ice into two periods: the melt period and the open water period. The results suggest that the total ice melting is primarily contributed by the ice basal melt (76%). Ice surface melt plays a minor role in ice variation. This indicates that atmosphere influences on the ice surface processes alone cannot explain ice variation, while oceanic heat fluxes that are influenced by atmosphere forcing and oceanic transport play a key role in ice basal processes and ice variation.

The heat budget estimation in the Kara Sea suggests that compared with lateral heat flux, vertical heat flux primarily regulates 96% and 79% of the heat budget in the water column during the melt and open water period, respectively. During the melt period, heat flux presents a significant correlation with T_{open} and is also suggested to dominate the interannual variation of the whole heat absorption process (r = 0.81, p < 0.01). The more heat input during this process leads to later T_{close} (r = 0.77, p < 0.01). Hence the heat flux during the melt period is crucial to the evolution of open water and can be a good indicator of DOW afterwards.

A link between T_{open} and DOW, i.e., DOW = $-1.72T_{open}$ + 177.15, is revealed based on satellite data. T_{open} is the number of days relative to the end of May. This prediction scheme for DOW via T_{open} supports earlier planning of marine activities. This study provides a reference for a profound understanding of the coupling effects of the positive feedback mechanism on the ocean-sea ice-air interaction in the marginal continental shelf where seasonal sea ice changes. With the future climate change in the Arctic Ocean, the prediction scheme is also sustainable if the seasonal sea ice still exists with ice coverage higher than 30% in the Kara Sea.

Acknowledgements

We acknowledge NSIDC (National Snow and Ice Data Centre of the USA National Oceanic and Atmospheric Administration) for providing the dataset of Climate Data Record of Passive Microwave Sea Ice Concentration (https://nsidc.org/data/G02202/versions/3). We are grateful to the NEMO development team for providing the state-of-the-art model. We also thank two anonymous reviewers for the very insightful and constructive comments that guided the revision of the manuscript.

References

Aksenov Y, Popova E E, Yool A, et al. 2017. On the future navigability of Arctic sea routes: High-resolution projections of the Arctic Ocean and sea ice. Marine Policy, 75: 300–317, doi: 10.1016/j.marpol.2015.12.027

Barnhart K R, Miller C R, Overeem I, et al. 2016. Mapping the future expansion of Arctic open water. Nature Climate Change, 6(3): 280–285, doi: 10.1038/nclimate2848

Belchansky G I, Douglas D C, Platonov N G. 2004. Duration of the Arctic Sea ice melt season: Regional and interannual variability, 1979–2001. Journal of Climate, 17(1): 67–80, doi: 10.1175/1520-0442(2004)017<0067:DOTASI>2.0.CO;2

Bird K J, Charpentier R R, Gautier D L, et al. 2008. Circum-arctic resource appraisal: Estimates of Undiscovered Oil and Gas North of the Arctic Circle. USGS Numbered Series 2008–3049. U.S. Geological Survey, 1–4

Bitz C M, Holland M M, Weaver A J, et al. 2001. Simulating the ice-thickness distribution in a coupled climate model. Journal of Geophysical Research: Oceans, 106(C2): 2441–2463, doi: 10.1029/1999jc000113

Blanchard-Wrigglesworth E, Armour K C, Bitz C M, et al. 2011. Persistence and inherent predictability of arctic sea ice in a GCM ensemble and observations. Journal of Climate, 24(1): 231–250, doi: 10.1175/2010JCLI3775.1

Bliss A C, Anderson M R. 2014. Daily area of snow melt onset on Arctic sea ice from passive microwave satellite observations 1979–2012. Remote Sensing, 6(11): 11283–11314, doi: 10.3390/rs61111283

Cavalieri D J, Gloersen P, Campbell W J. 1984. Determination of sea ice parameters with the Nimbus 7 SMMR. Journal of Geophysical Research: Atmospheres, 89(D4): 5355–5369, doi: 10.1029/JD089iD04p05355

Cavalieri D J, Parkinson C L. 2012. Arctic sea ice variability and trends, 1979–2010. The Cryosphere, 6(4): 881–889, doi: 10.5194/tc-6-881-2012

Chen Ping, Zhao Jinping. 2017. Impacts of surface wind on regional and integrated changes of sea ice in the Arctic. Periodical of Ocean University of China (in Chinese), 47(8): 1–12, doi: 10.16441/j.cnki.hdxb.20160212

Comiso J C. 1986. Characteristics of Arctic winter sea ice from satellite multispectral microwave observations. Journal of Geophysical Research: Oceans, 91(C1): 975–994, doi: 10.1029/JC091iC01p00975

Comiso J C, Nishio F. 2008. Trends in the sea ice cover using enhanced and compatible AMSR-E, SSM/I, and SMMR data. Journal of Geophysical Research: Oceans, 113(2): C02S07, doi: 10.1029/2007JC004257

Curry J A, Schramm J L, Ebert E E. 1995. Sea ice-albedo climate feedback mechanism. Journal of Climate, 8(2): 240–247, doi: 10.1175/1520-0442(1995)008<0240:SIACFM>2.0.CO;2

Dmitrenko I A, Rudels B, Kirillov S A, et al. 2015. Atlantic water flow into the Arctic Ocean through the St. Anna Trough in the northern Kara Sea. Journal of Geophysical Research: Oceans, 120(7): 5158–5178, doi: 10.1002/2015JC010804

Duan Chenglin, Dong Sheng, Wang Zhifeng. 2019a. Sea ice regime in the Kara Sea during 2003–2017 based on high-resolution satellite data. Polish Polar Research, 40(3): 205–225, doi: 10.24425/ppr.2019.129671

Duan Chenglin, Dong Sheng, Xie Zexiao, et al. 2019b. Temporal variability and trends of sea ice in the Kara Sea and their relationship with atmospheric factors. Polar Science, 20: 136–147, doi: 10.1016/j.polar.2019.03.002

Flanner M G, Shell K M, Barlage M, et al. 2011. Radiative forcing and albedo feedback from the Northern Hemisphere cryosphere between 1979 and 2008. Nature Geoscience, 4(3): 151–155, doi: 10.1038/ngeo1062

Gautier D L, Bird K J, Charpentier R R, et al. 2009. Assessment of undiscovered oil and gas in the Arctic. Science, 324(5931): 1175–1179, doi: 10.1126/science.1169467

Hu Xianmin, Sun Jiangfan, Chan T O, et al. 2018. Thermodynamic and dynamic ice thickness contributions in the Canadian Arctic Archipelago in NEMO-LIM2 numerical simulations. The Cryosphere, 12(4): 1233–1247, doi: 10.5194/tc-12-1233-2018

Ikeda M, Wang Jiang, Zhao Jinping. 2011. Hypersensitive decadal oscillations in the Arctic/subarctic climate. Geophysical Research Letters, 28(7): 1275–1278, doi: 10.1029/2000GL011773

Johnson M A, Eicken H. 2016. Estimating Arctic sea-ice freeze-up and break-up from the satellite record: A comparison of different approaches in the Chukchi and Beaufort Seas. Elementa-Sci-

ence of the Anthropocene, 4: 000124, doi: 10.12952/journal.elementa.000124

Kern S, Harms I, Bakan S, et al. 2005. A comprehensive view of Kara Sea polynya dynamics, sea-ice compactness and export from model and remote sensing data. Geophysical Research Letters, 32(15): L15501, doi: 10.1029/2005GL023532

Kim K Y, Hamlington B D, Na H N, et al. 2016. Mechanism of seasonal Arctic sea ice evolution and Arctic amplification. The Cryosphere, 10(5): 2191–2202, doi: 10.5194/tc-10-2191-2016

Lebrun M, Vancoppenolle M, Madec G, et al. 2019. Arctic sea-ice-free season projected to extend into autumn. The Cryosphere, 13(1): 79–96, doi: 10.5194/tc-13-79-2019

Lei Ruibo, Tian-Kunze X, Leppäranta M, et al. 2016. Changes in summer sea ice, albedo, and portioning of surface solar radiation in the Pacific sector of Arctic Ocean during 1982–2009. Journal of Geophysical Research: Oceans, 121(8): 5470–5486, doi: 10.1002/2016JC011831

Lei Ruibo, Xie Hongjie, Wang Jia, et al. 2015. Changes in sea ice conditions along the Arctic Northeast Passage from 1979 to 2012. Cold Regions Science and Technology, 119: 132–144, doi: 10.1016/j.coldregions.2015.08.004

Leifer I, Chen F R, McClimans T, et al. 2018. Satellite ice extent, sea surface temperature, and atmospheric methane trends in the Barents and Kara seas. The Cryosphere Discuss, 1–45, doi: 10.5194/tc-2018-75

Lien V S, Schlichtholz P, Skagseth Ø, et al. 2017. Wind-driven atlantic water flow as a direct mode for reduced barents sea ice cover. Journal of Climate, 30(2): 803–812, doi: 10.1175/jcli-d-16-0025.1

Lindsay R, Schweiger A. 2015. Arctic sea ice thickness loss determined using subsurface, aircraft, and satellite observations. The Cryosphere, 9(1): 269–283, doi: 10.5194/tc-9-269-2015

Lindsay R W, Zhang Jinlun. 2005. The thinning of Arctic Sea Ice, 1988–2003: have we passed a tipping point?. Journal of Climate, 18(22): 4879–4894, doi: 10.1175/JCLI3587.1

Luo Xiaofan, Hu Xianmin, Nie Hongtao, et al. 2019. Evaluation of hindcast simulation with the ocean and sea-ice model covering the Arctic and adjacent oceans. Haiyang Xuebao (in Chinese), 41(9): 1–12, doi: 10.3969/j.issn.0253-4193.2019.09.001

Madec G. 2008. NEMO ocean engine, version 3.6. Note du Pôle de Modélisation, Institut Pierre-Simon Laplace, 27: 386

Madec G, Imbard M. 1996. A global ocean mesh to overcome the North Pole singularity. Climate Dynamics, 12(6): 381–388, doi: 10.1007/BF00211684

Markus T, Stroeve J C, Miller J. 2009. Recent changes in Arctic sea ice melt onset, freezeup, and melt season length. Journal of Geophysical Research: Oceans, 114(C12): C12024, doi: 10.1029/2009JC005436

Maslanik J A, Serreze M C, Barry R G. 1996. Recent decreases in Arctic summer ice cover and linkages to atmospheric circulation anomalies. Geophysical Research Letters, 23(13): 1677–1680, doi: 10.1029/96GL01426

Meier W N, Fetterer F, Duerr R, et al. 2017. NOAA/NSIDC climate data record of passive microwave sea ice concentration, Version 3. Boulder, Colorado USA. NSIDC: National Snow and Ice Data Center, doi: 10.7265/N59P2ZTG

Mysak L A, Venegas S A. 1998. Decadal climate oscillations in the Arctic: A new feedback loop for atmosphere-ice-ocean interactions. Geophysical Research Letters, 25(19): 3607–3610, doi: 10.1029/98GL02782

Navy's Task Force Climate Change. 2014. The United States navy arctic roadmap for 2014 to 2030. Washington, D C: University of North Texas Libraries, UNT Digital Library

Ogi M, Rigor I G, McPhee M G, et al. 2008. Summer retreat of Arctic sea ice: Role of summer winds. Geophysical Research Letters, 35(24): L24701, doi: 10.1029/2008GL035672

Onarheim I H, Eldevik T, Smedsrud L H, et al. 2018. Seasonal and regional manifestation of arctic sea ice loss. Journal of Climate, 31(12): 4917–4932, doi: 10.1175/JCLI-D-17-0427.1

Osadchiev A A, Izhitskiy A S, Zavialov P O, et al. 2017. Structure of the buoyant plume formed by Ob and Yenisei river discharge in the southern part of the Kara Sea during summer and autumn. Journal of Geophysical Research: Oceans, 122(7): 5916–5935, doi: 10.1002/2016JC012603

Perovich D K, Light B, Eicken H, et al. 2007b. Increasing solar heating of the Arctic Ocean and adjacent seas, 1979–2005: Attribution and role in the ice-albedo feedback. Geophysical Research Letters, 34(19): L19505, doi: 10.1029/2007GL031480

Perovich D K, Nghiem S V, Markus T, et al. 2007a. Seasonal evolution and interannual variability of the local solar energy absorbed by the Arctic sea ice-ocean system. Journal of Geophysical Research: Oceans, 112(3): C03005, doi: 10.1029/2006JC003558

Polyakov I V, Alekseev G V, Bekryaev R V, et al. 2003. Long-term ice variability in Arctic marginal seas. Journal of Climate, 16(12): 2078–2085, doi: 10.1175/1520-0442(2003)016<2078:LIVIAM>2.0.CO;2

Rigor I G, Wallace J M, Colony R L. 2002. Response of sea ice to the Arctic oscillation. Journal of Climate, 15(18): 2648–2663, doi: 10.1175/1520-0442(2002)015<2648:ROSITT>2.0.CO;2

Rousset C, Vancoppenolle M, Madec G, et al. 2015. The Louvain-La-Neuve sea ice model LIM3.6: global and regional capabilities. Geoscientific Model Development, 8(10): 2991–3005, doi: 10.5194/gmd-8-2991-2015

Screen J A, Simmonds I. 2010. The central role of diminishing sea ice in recent Arctic temperature amplification. Nature, 464(7293): 1334–1337, doi: 10.1038/nature09051

Serreze M C, Barry R G. 2011. Processes and impacts of Arctic amplification: A research synthesis. Global and Planetary Change, 77(1–2): 85–96, doi: 10.1016/j.gloplacha.2011.03.004

Serreze M C, Crawford A D, Stroeve J C, et al. 2016. Variability, trends, and predictability of seasonal sea ice retreat and advance in the Chukchi Sea. Journal of Geophysical Research: Oceans, 121(10): 7308–7325, doi: 10.1002/2016JC011977

Simmonds I. 2015. Comparing and contrasting the behaviour of Arctic and Antarctic sea ice over the 35 year period 1979–2013. Annals of Glaciology, 56(691): 18–28, doi: 10.3189/2015AoG69A909

Stammerjohn S, Massom R, Rind D, et al. 2012. Regions of rapid sea ice change: An inter-hemispheric seasonal comparison. Geophysical Research Letters, 39(6): L06501, doi: 10.1029/2012GL050874

Stroeve J C, Crawford A D, Stammerjohn S. 2016. Using timing of ice retreat to predict timing of fall freeze-up in the Arctic. Geophysical Research Letters, 43(12): 6332–6340, doi: 10.1002/2016GL069314

Stroeve J C, Markus T, Boisvert L, et al. 2014. Changes in Arctic melt season and implications for sea ice loss. Geophysical Research Letters, 41(4): 1216–1225, doi: 10.1002/2013GL058951

Stroeve J C, Notz D. 2018. Changing state of Arctic sea ice across all seasons. Environmental Research Letters, 13(10): 3001, doi: 10.1088/1748-9326/aade56

Uotila P, Iovino D, Vancoppenolle M, et al. 2017. Comparing sea ice, hydrography and circulation between NEMO3.6 LIM3 and LIM2. Geoscientific Model Development, 10(2): 1009–1031, doi: 10.5194/gmd-10-1009-2017

Vancoppenolle M, Fichefet T, Goosse H, et al. 2009. Simulating the mass balance and salinity of Arctic and Antarctic sea ice. 1. Model description and validation. Ocean Modelling, 27(1–2): 33–53, doi: 10.1016/j.ocemod.2008.10.005

Wang Yali, Luo Xiaofan, Zhang Yongli, et al. 2019a. Heat budget analysis during the ice-melting season in the Chukchi Sea based on a model simulation. Chinese Science Bulletin (in Chinese), 64(33): 3485–3497, doi: 10.1360/N972019-00322

Wang Yunhe, Bi Haibo, Huang Haijun, et al. 2019b. Satellite-observed trends in the Arctic sea ice concentration for the period 1979–2016. Journal of Oceanology and Limnology, 37(1): 18–37,

doi: 10.1007/s00343-019-7284-0

Woodgate R A. 2018. Increases in the Pacific inflow to the Arctic from 1990 to 2015, and insights into seasonal trends and driving mechanisms from year-round Bering Strait mooring data. Progress in Oceanography, 160: 124–154, doi: 10.1016/j.pocean.2017.12.007

Woodgate R A, Stafford K M, Prahl F G. 2015. A synthesis of year-round interdisciplinary mooring measurements in the bering strait (1990–2014) and the RUSALCA Years (2004–2011). Oceanography, 28(3SI): 46–67, doi: 10.5670/oceanog.2015.57

Zhang Jinlun, Rothrock D, Steele M. 2000. Recent changes in Arctic sea ice: The interplay between ice dynamics and thermodynamics. Journal of Climate, 13(17): 3099–3114, doi: 10.1175/1520-0442(2000)013<3099:RCIASI>2.0.CO;2

Zhang Yongli, Wei Hao, Lu Youyu, et al. 2020. Dependence of Beaufort Sea low ice condition in the summer of 1998 on ice export in the prior winter. Journal of Climate, 33(21): 9247–9259, doi: 10.1175/jcli-d-19-0943.1